


## Article

# Influence of Alumina Nanofibers Sintered by the Spark Plasma Method on Nickel Mechanical Properties

Leonid Agureev <sup>1,\*</sup> , Valeriy Kostikov <sup>2</sup>, Zhanna Ereemeeva <sup>2</sup>, Svetlana Savushkina <sup>1</sup>, Boris Ivanov <sup>1</sup>, Dmitriy Khmelenin <sup>3</sup>, Gleb Belov <sup>4</sup> and Yuri Solyaev <sup>5</sup>

<sup>1</sup> Keldysh Research Center, 125438 Moscow, Russia; sveta\_049@mail.ru (S.S.); ibs@live.ru (B.I.)

<sup>2</sup> Department of Powder Metallurgy and Functional Coatings, National University of Science and Technology "MISIS", 119991 Moscow, Russia; technosteel@mail.ru (V.K.); eremeeva-shanna@yandex.ru (Z.E.)

<sup>3</sup> Shubnikov Institute of Crystallography of Federal Scientific Research Centre "Crystallography and Photonics" of Russian Academy of Sciences, 119333 Moscow, Russia; xorrunn@gmail.com

<sup>4</sup> Joint Institute for High Temperatures of the Russian Academy of Sciences, 125412 Moscow, Russia; gbelov@yandex.ru

<sup>5</sup> Institute of Applied Mechanics of Russian Academy of Sciences, 125040 Moscow, Russia; yurysolyaev@yandex.ru

\* Correspondence: trynano@gmail.com; Tel.: +7-903-723-7969

**Abstract:** The article presents the study of alumina nanoparticles' (nanofibers) concentration effect on the strength properties of pure nickel. The samples were obtained by spark plasma sintering of previously mechanically activated metal powders. The dependence of the grain size and the relative density of compacts on the number of nanofibers was investigated. It was found that with an increase in the concentration of nanofibers, the average size of the matrix particles decreased. The effects of the nanoparticle concentration (0.01–0.1 wt.%) on the elastic modulus and tensile strength were determined for materials at 25 °C, 400 °C, and 750 °C. It was shown that with an increase in the concentration of nanofibers, a 10–40% increase in the elastic modulus and ultimate tensile strength occurred. A comparison of the mechanical properties of nickel in a wide range of temperatures, obtained in this work with materials made by various technologies, is carried out. A description of nanofibers' mechanisms of influence on the structure and mechanical properties of nickel is given. The possible impact of impurity phases on the properties of nickel is estimated. The tendency of changes in the mechanical properties of nickel, depending on the concentration of nanofibers, is shown.

**Keywords:** nanofibers; powder metallurgy; spark plasma sintering; elastic modulus; tensile strength; nickel



**Citation:** Agureev, L.; Kostikov, V.; Ereemeeva, Z.; Savushkina, S.; Ivanov, B.; Khmelenin, D.; Belov, G.; Solyaev, Y. Influence of Alumina Nanofibers Sintered by the Spark Plasma Method on Nickel Mechanical Properties. *Metals* **2021**, *11*, 548. <https://doi.org/10.3390/met11040548>

Academic Editor: Eric Hug

Received: 22 February 2021

Accepted: 25 March 2021

Published: 28 March 2021

**Publisher's Note:** MDPI stays neutral with regard to jurisdictional claims in published maps and institutional affiliations.



**Copyright:** © 2021 by the authors. Licensee MDPI, Basel, Switzerland. This article is an open access article distributed under the terms and conditions of the Creative Commons Attribution (CC BY) license (<https://creativecommons.org/licenses/by/4.0/>).

## 1. Introduction

Nickel-based materials are used in various industries: aviation, astronautics, engineering, energy, and others [1]. Nickel is a universal chemically stable metal. Nickel strengthening can be associated with a wide range of different methods [2]: Peirls–Nabarro strengthening, solid solution strengthening, dislocation strengthening, dispersion strengthening, and grain boundary strengthening. Pure nickel is not used as a structural material because of its high density and relatively low strength. However, its modification allows one to achieve a significant increase in mechanical properties [3].

Dispersion strengthening of metals is caused by both coherent and incoherent particles and precipitates. There are many works related to the strengthening of molybdenum [4] and aluminum [5–7] by 0.01–0.1 wt.% spherical nanoparticles of refractory oxides. It was shown that the increase in tensile strength could reach 30–300% compared to pure metal. Materials were obtained using powder metallurgy technologies. The addition of nanoparticles into a powder matrix leads to various strengthening effects:

- grain refinement;
- prevents boundaries from growing and moving;

- increases the yield strength and breaking stress, maintaining the distance between matrix grains [8–11];
- contributes to strengthening by the double grain boundaries mechanism [10,12];
- inhibits creep along the grain boundaries, thru indenting into the matrix and turning with crack propagation process [9,13];
- limits the nucleation and promotes the vacancies annihilation, increasing the creep resistance along the grain boundaries [14];
- prevents the diffusion of oxidizer due to adsorption on the nanoparticles surface [8].

Usually, materials based on nickel are obtained by casting or powder metallurgy. The main advantage of spark plasma sintering (SPS) is the possibility of rapid powder consolidation with the preservation of the initial particle sizes [15,16]. Powder materials can significantly differ in properties when compared to cast materials. For example, in the literature [17], nickel powders of various particle sizes and morphologies were used for materials' production by the SPS method. Both nanosized ( $\sim 10$  nm) and bimodal-sized ( $\sim 15$   $\mu\text{m}$ ) particles were used. The tensile strength of sintered samples was in the range of 500–650 MPa. The samples' microstructure was distinguished by the presence of small grains (below 2  $\mu\text{m}$ ) and large grains with a size of 10–25  $\mu\text{m}$ . In the literature [18], nickel powders with a particle size of 52–250 nm were ground in a planetary mill and sintered by SPS. The tensile strength of this material was 680–700 MPa.

It should be noted that the addition of refractory insoluble high-modulus nanoparticles into the metal matrix in small quantities (up to 0.1 wt.%) contributes to their more straightforward and more uniform distribution [19,20]. This is because nanoparticles are prone to aggregation. According to the Obraztsov–Lurie–Belov micromechanical model based on the gradient theory of elasticity [5], a rigid nanoparticle, being in a soft matrix, contributes to the formation of an interphase strengthening zone, characterized by increased mechanical characteristics compared to the matrix. The better the nanoparticles are distributed, the more uniform and continuous these zones are. In this case, the metal, as noted above, can significantly harden. A preliminary theoretical estimate of the interfacial layer size, made using the gradient model of the interfacial layer in elasticity theory [21], shows that its relative value is approximately equal to  $l_0/r_0 = 7\text{--}10$ , where  $r_0$  is the spherical nanoinclusions radius (in this case, the radius of the cylinder base) (Figure 1).

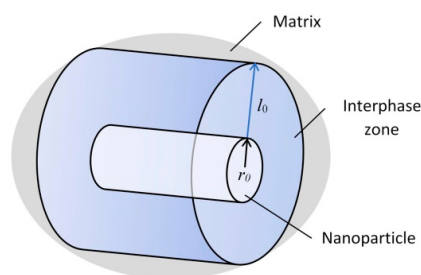


**Figure 1.** The structure of the interfacial zone of strengthening around nanoinclusions.

## 2. Materials and Methods

In this study, pure nickel has been modified by introducing alumina nanofibers. PNK-UT3 nickel powder (3–5  $\mu\text{m}$ , 99.9% Ni, OJSC MMC Norilsk Nickel, Norilsk, Russia) was used as a matrix. Nafen<sup>TM</sup> alumina nanofibers (Nf, ANF Technology, Tallin, Estonia) were used for modification (diameter  $\sim 10$  nm, length up to 5  $\mu\text{m}$ ) [22]. Alumina nanofibers have beneficial properties that make them an excellent hardener for metals. They have a high tensile strength (up to 12 GPa), thermal stability of up to 1200  $^{\circ}\text{C}$ , a faceted surface for better bonding with the matrix, and a high modulus of elasticity (400 GPa) [23,24].

The activation of nickel powder was carried out in a planetary mill “Activator-2SL” (LLC “Plant of Chemical Engineering”, s. Dorogino, Russia) in steel jars for 20 min in Ar atmosphere. Stainless steel grinding balls with a diameter of 5 mm and a ratio of Powder:Ball = 1:10 were used (Hunan Togoal Instrument & Equipment Co., Ltd., Hunan,

China). Activation was carried out in isopropyl alcohol of chemical purity with a 0.1 wt.% surfactant addition. During the mechanical activation, iron was ground from the balls. Before grinding, the nickel powder was stirred with steel balls for 20 h to form a protective nickel layer on them and the jars' walls. This technique is confirmed by several works [25,26]. The source [27] said that the fact that the amount of iron in nickel is up to 0.25 wt.% does not significantly affect the properties.

The particle size distribution before and after grinding was investigated on a Microtrac S 3500 unit.

Nanoparticles of alumina fibers were dispersed in isopropyl alcohol using a UPS 3600 Sonoplus ultrasonic homogenizer (BANDELIN electronic GmbH & Co. KG, Berlin, Germany) for 3 min at a power level of 50% in pulsed mode. The addition of nanoparticles in nickel powder was carried out in isopropyl alcohol under the influence of a low-power ultrasound in an ultrasonic bath for 5 min while stirring the solution with an overhead stirrer at a speed of 400 rpm. Then, it was dried in a vacuum oven at 250 °C for 10 h. After that, the powder was sintered in a graphite mold in tablets with a diameter of 30 mm and a height of 3 mm by a spark plasma sintering method using the FCT Systeme GmbH installation (Rauenstein, Germany). The sintering temperature was 950 °C, the duration time was 20 min, the heating rate was 95°/min, the cooling rate was 45°/min, the process was carried out in argon, and the pressing pressure was 50 MPa (pressing stages were: 25 MPa—first 10 min, 50 MPa—last 10 min). Samples were obtained with a concentration of nanoparticles equal to 0, 0.01, 0.025, 0.05, 0.075, and 0.1 wt.%.

The tensile tests were done using plane samples (overall length of 25 mm, thickness of 3 mm, width of 10 mm, and width of grip section of 5 mm) at 25 °C, 400 °C, and 750 °C on a universal installation for mechanical testing TestSystems-VacEto (Keldysh Research Center, VacEto LLC, Moscow, Russia). The Young's modulus of nickel with the addition of nanoparticles was determined by a MUZA ultrasonic machine at temperatures of 25 °C, 400 °C, and 750 °C. For this, rectangles 5 × 15 × 3 mm in size were cut from each tablet.

The structure of the samples was investigated using a Quanta 600 scanning electron microscope (FEI Company, Hillsboro, OR, USA). The fine structure and composition were examined with a transmission electron microscope FEI Osiris (Shubnikov Institute of Crystallography, FEI Company, Hillsboro, OR, USA).

### 3. Results

#### 3.1. Microstructure

Figure 2 shows the nickel particles size distribution before and after mechanical activation in a planetary mill. Nickel particles after activation had a more uniform size distribution compared to untreated powder. This is illustrated by the fact that powders with a size of 20 µm or more were ground to 10 µm or less.

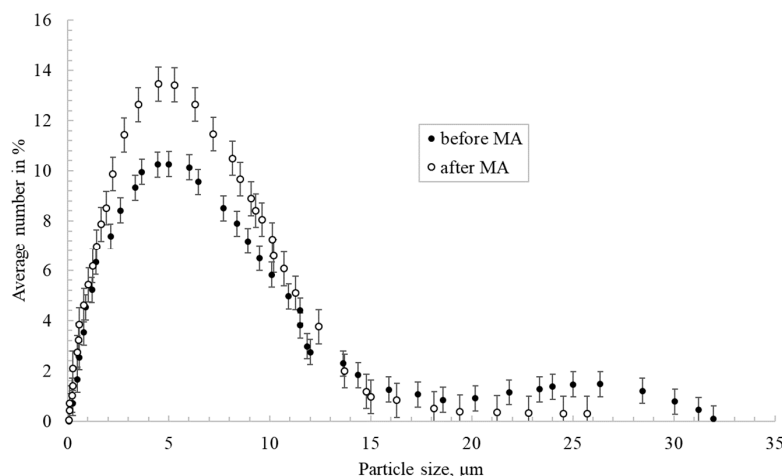
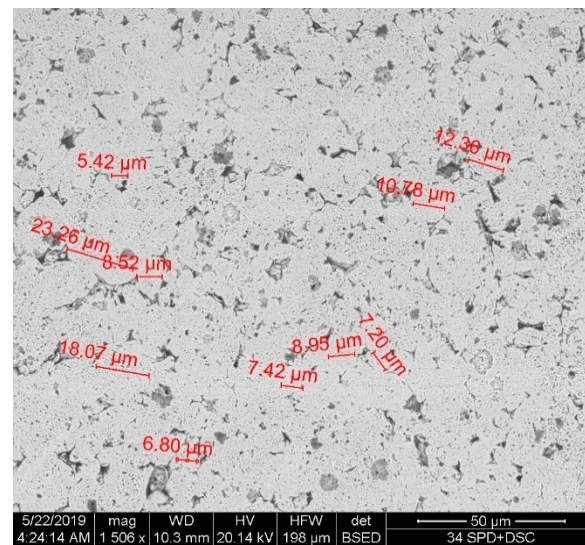


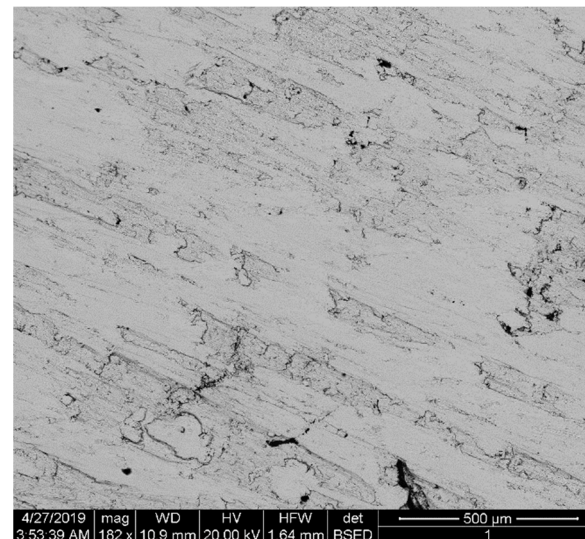
Figure 2. Nickel particles' size distribution before and after mechanical activation (MA).

Figure 3 shows the microstructure of the sintered nickel samples without nanofibers and with 0.1 wt.% nanofibers. Samples were etched with a solution of  $\text{HNO}_3 + \text{H}_2\text{O} + \text{CH}_3\text{COOH}$ . Figure 3a shows the microstructure surface of a sintered nickel without nanofibers. Figure 3b,c shows the microstructure surface of a sintered nickel sample with 0.1 wt. % nanofibers.

The average size of nickel grains depending on the nanofibers' concentration (Figure 4) was determined by the secant method. With an increase of the nanofibers' concentration, the average grain size decreases significantly compared to pure sintered nickel from 8 to 3  $\mu\text{m}$ . This is due to the fact that nanofibers are playing the role of obstacles to the recrystallization of nickel grains during sintering.

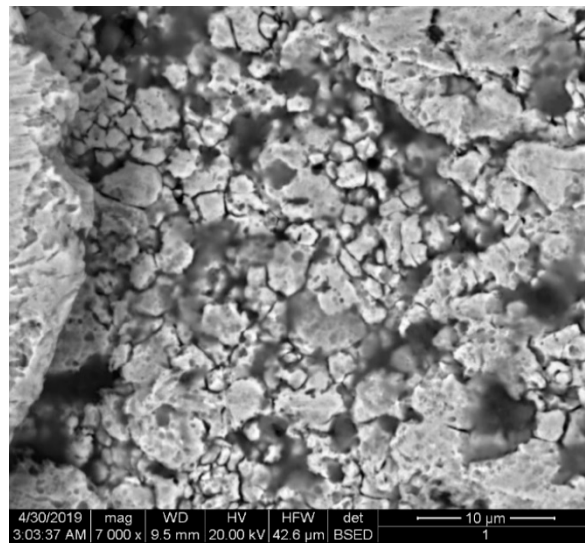


(a)



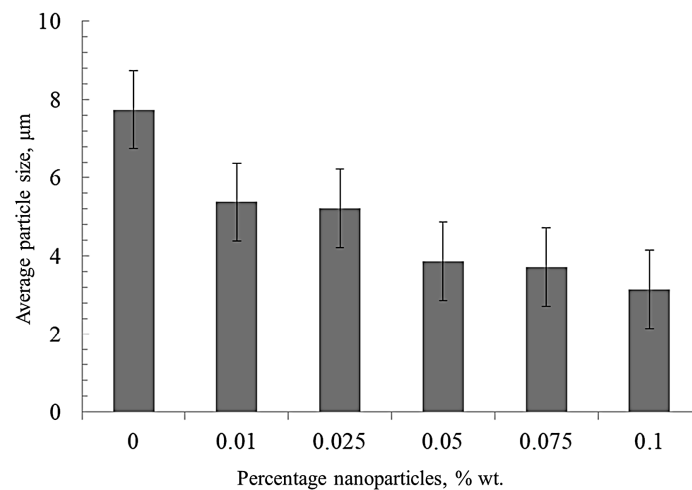
(b)

Figure 3. Cont.



(c)

**Figure 3.** The microstructure of the sintered nickel samples: (a) Surface of nickel without nanofibers; (b,c) Surface of nickel with 0.1 wt.% nanofibers at different magnifications.



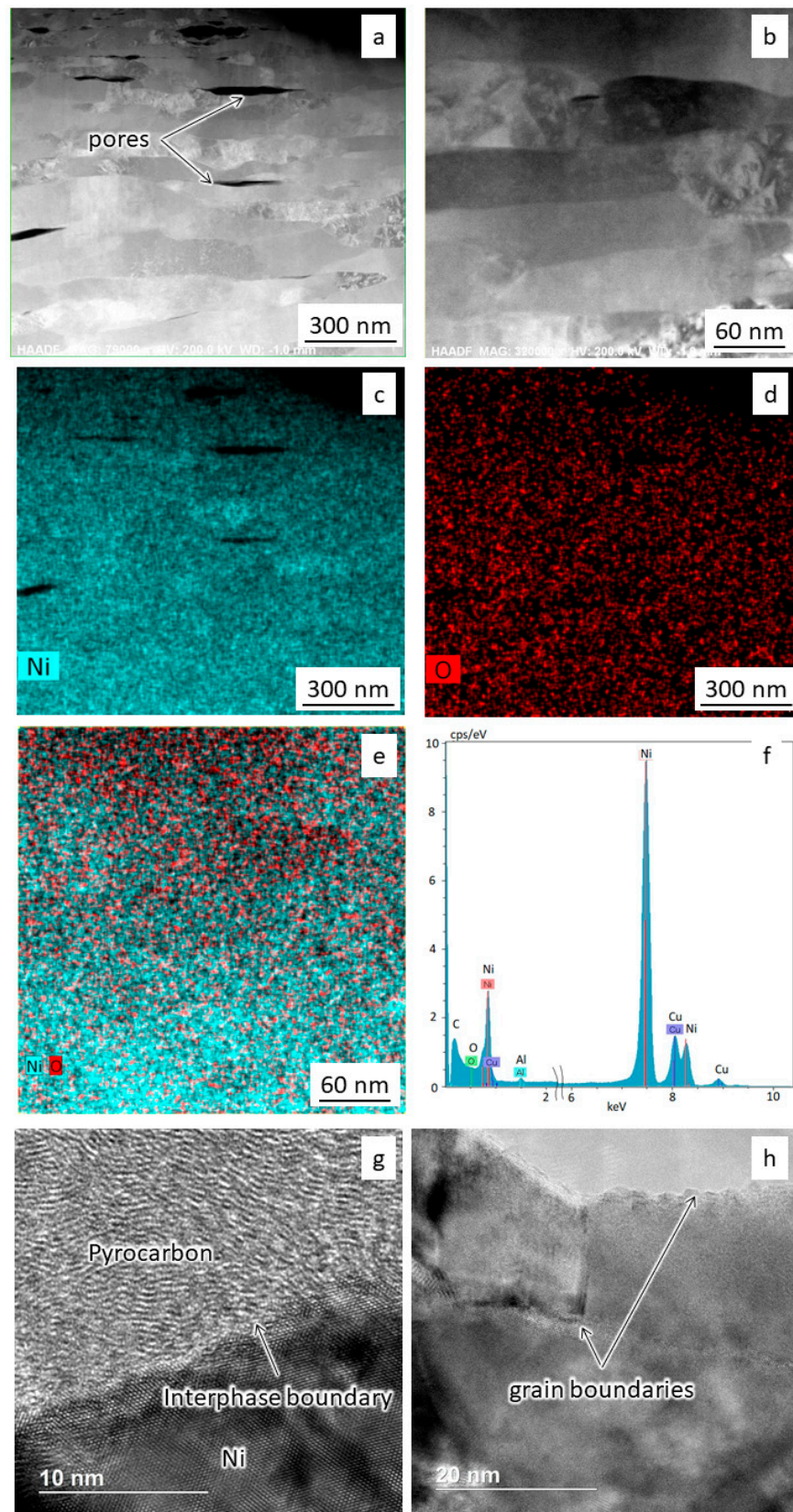
**Figure 4.** The effect of the nanofibers' concentration on the average grain size of nickel.

The images in Figures 5–7 show the results of transmission electron microscopy (TEM) microscopy of the sintered nickel without and with an addition of 0.1 wt.% nanofibers.

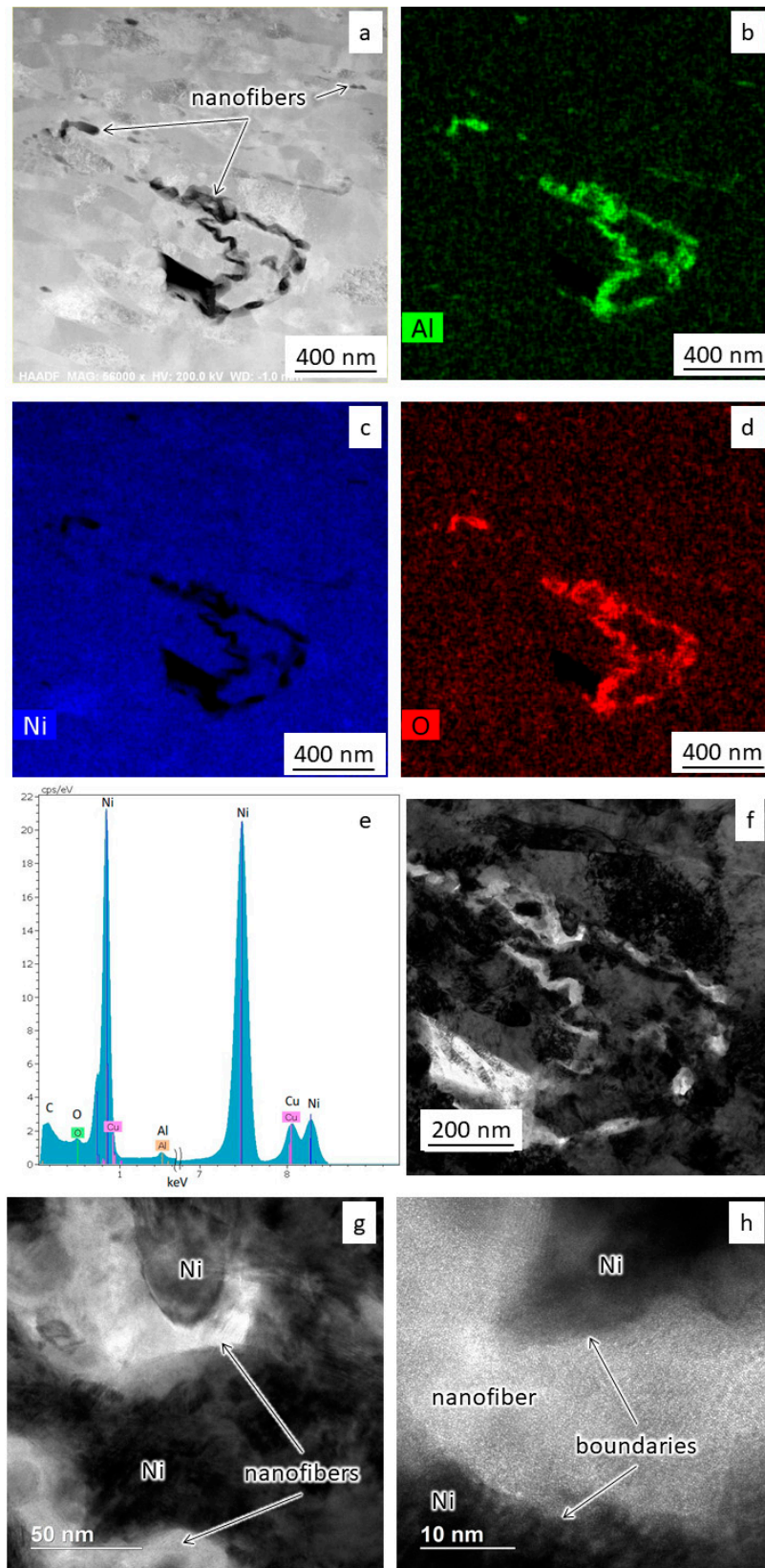
It was found that the nickel samples contained elongated submicron grains 50–70 nm wide and more than 200 nm long (Figure 5a,b). According to spectral mapping analysis results, the samples contain nickel and a small amount of oxygen on the surface (Figure 5c–f). Figure 5g shows carbon formed during spark plasma sintering, which can contribute to the hardening of nickel. The unnamed peak in Figure 5f on the left is from surface carbon pollution. The copper peak refers to the holder material. The grain boundaries are clean and have no visible oxide layers (Figure 5g,h).

Figure 6a shows a bright-field image of the modified material microstructure. Nickel grains also have an elongated shape with a width of more than 50 nm and a length of more than 200 nm. Spectral mapping and dark-field imaging (Figure 6b–f) show alumina nanofibers' presence along the grain boundaries of the nickel. The length of nanofibers varies from 300 to 1000 nm. One can also see no additional oxide layers between the nanofibers and nickel grains (Figure 6g,h).





**Figure 5.** TEM studies of sintered nickel: (a,b) Microstructure at different magnifications; (c–f) Spectral analysis results; (g,h) Grain boundary structure.



**Figure 6.** The results of TEM studies of sintered nickel with 0.1 wt.% nanofibers: (a) Grains' microstructure; (b–e) Results of spectral analysis; (f) The dark-field image of the microstructure; (g,h) The structure of the interfaces.



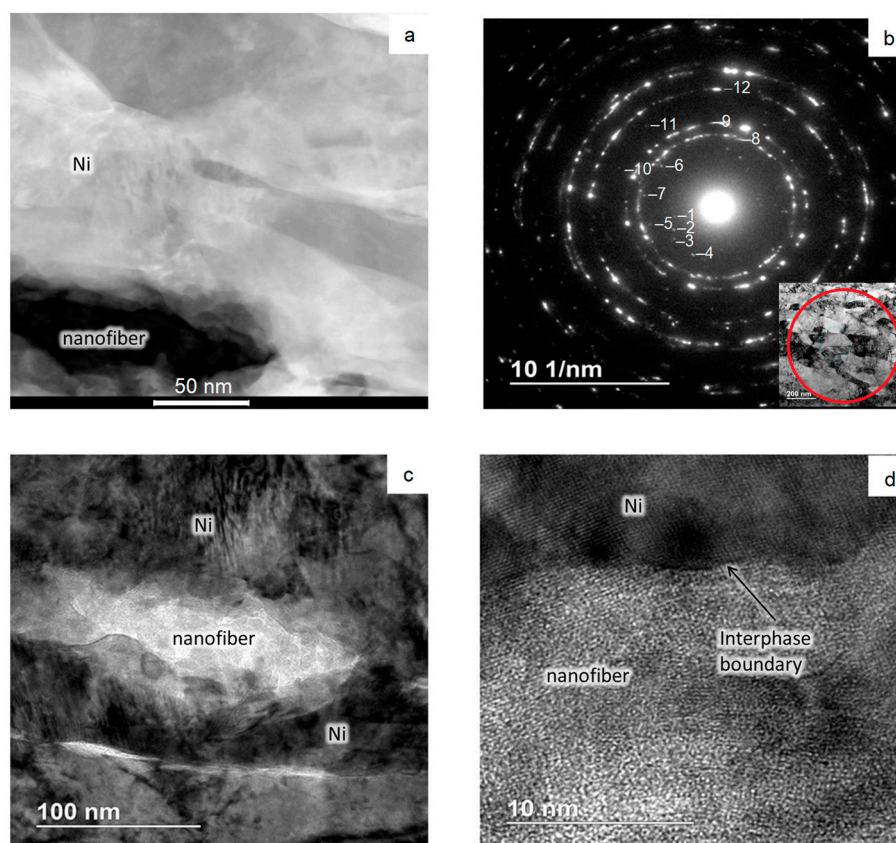


**Figure 7.** Results of TEM studies of the area with nanofibers: (a) Grains' microstructure; (b) Diffraction pattern; (c,d) The structure of the interphase layer.

Figure 7 shows high-magnification images of the structure and a diffraction pattern. Nanoparticles have an elongated shape with curved faceted boundaries (Figure 7a,c). The boundary between the nanofiber and the matrix appears to be exact (Figure 7d). The diffraction pattern, taken from the sample area in Figure 7a, shows that the material is polycrystalline (Figure 7b). It looks like there are phases that may be contained in sintered material, like  $\text{Al}_2\text{O}_3$  (rings №№ 1, 2, 4–7, 10–12), Ni (rings №№ 7–10, 12), and NiO (rings №№ 11, 12).

### 3.2. Elastic properties

Figure 8 shows that the modified materials' Young's modulus trend changes depending on the nanofibers' concentration and test temperature. The module's growth at room temperature was 1–10% for nickel with different nanofiber contents when compared with "pure" nickel.

The elastic properties behavior of SPS-sintered nickel looks interesting, both without and with nanofibers. Figure 9 shows the change in Young's modulus of nickel depending on the composition compared with cast samples produced by other researchers [27–30]. The elastic modulus of nickel with nanofibers is higher than that of unmodified materials over practically the entire test temperature range. Furthermore, it should be clarified that the nickel studied by Farraro [28] was annealed (tempered) at 1000 °C for 20 h. Koster [30] investigated nickel tempered at 900 °C. Orlov and Fedotov [30] used 99.98% nickel.



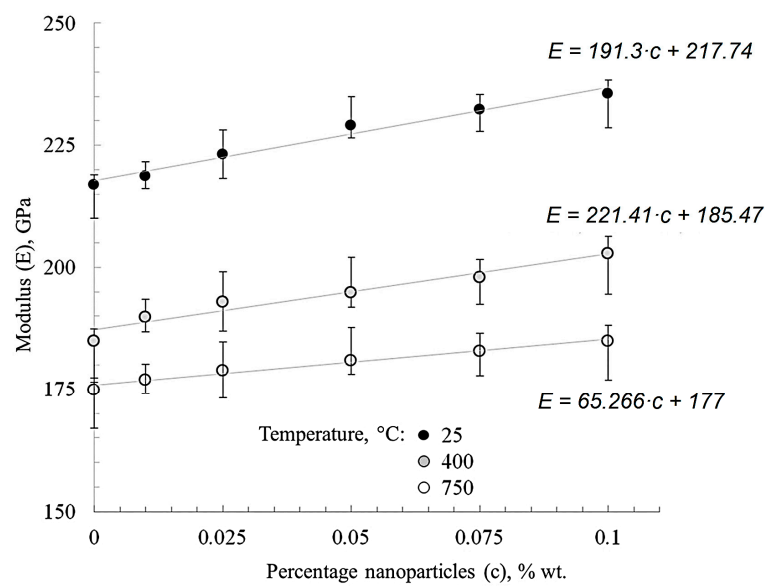


**Figure 8.** The effect of nanofibers' concentration and test temperature on the elastic modulus of nickel.

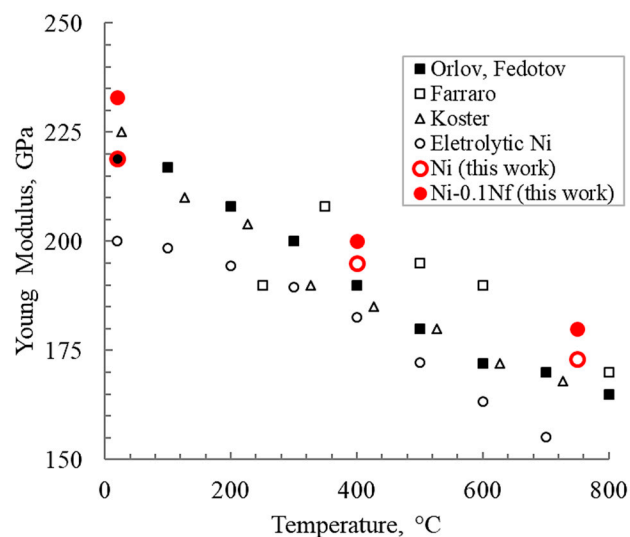
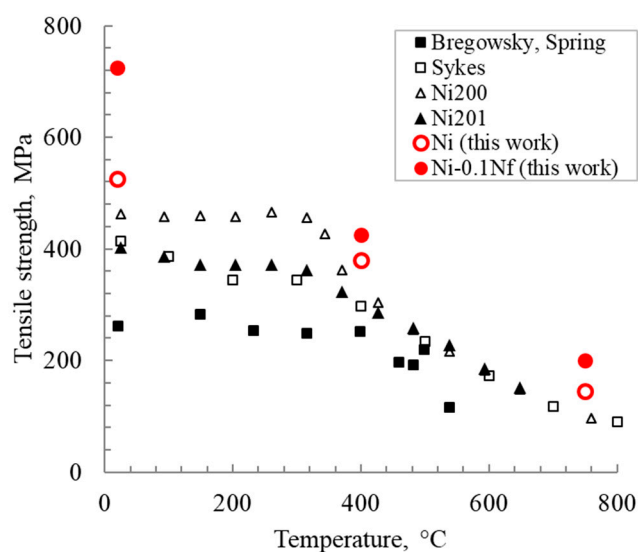


**Figure 9.** Young's modulus depending on the temperature for different manufacturing methods.

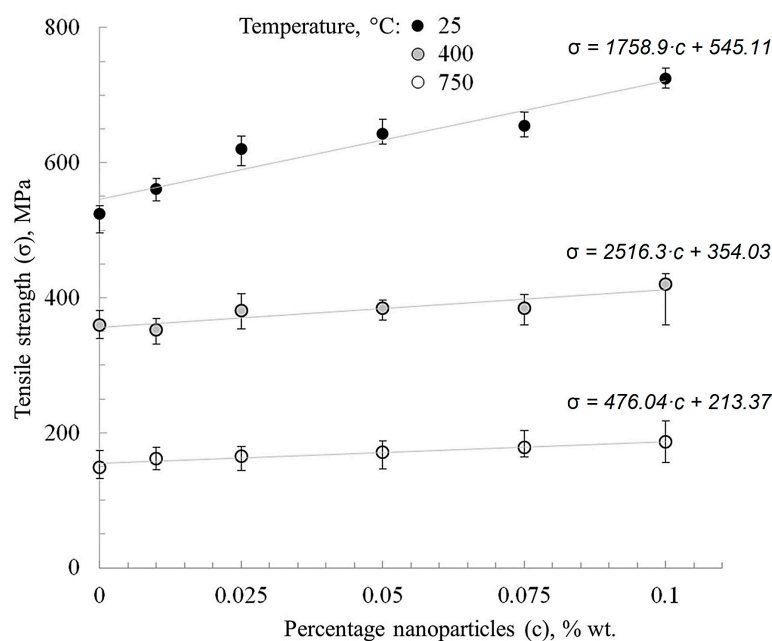
### 3.3. Tensile Strength

Figure 10 shows the temperature dependences of the tensile strength for Ni and Ni-0.1Nf alloys in comparison with materials obtained in other works [27]. Nickel with nanofibers demonstrates a tensile strength increase throughout the entire test temperature range. At 750 °C, this trend becomes less noticeable. To clarify, Bregowsky and Spring [27,30] used cast nickel. Sykes investigated tempered nickel at 800 °C as rolled wire (99.8% Ni, 0.15% Fe, and Co), and Ni200 and Ni201 were also tempered [29].

In this regard, alumina nanofibers prevent high-temperature creep when the matrix still retains strength properties. At 750 °C, the metal softens significantly, recrystallizes, and the action of nanofibers located at the grain boundaries slows down the deformation processes. Figure 11 shows the effect of nanofibers' concentration and test temperature on nickel strength. It is known that the rate of high-temperature deformation depends on the microstructure [14]. High-strength and melting-point nanoparticles could help slow the deformation, playing roles as dislocation stoppers and vacancy annihilators.



**Figure 10.** The tensile strength of nickel depending on the temperature for different nickel manufacturing methods.



**Figure 11.** Effect of nanofibers' concentration and test temperature on nickel strength.

Figure 11 shows that nanofibers' addition affects the strength of nickel, especially at temperatures of up to 400 °C. This is associated with the inhibition of nickel, primarily recrystallization, which usually takes place at temperatures of 250–400 °C, according to the Bollman diagram [31]. During the statistical processing of the strength-concentration plots, it was noted that the tendency for nickel hardening modified with aluminum oxide nanofibers persists over the entire test temperature range (25–750 °C).

Figure 12 shows a tendentious relationship between the strength, Young's modulus, and nanoparticle concentration at various test temperatures of nickel samples. As noted above, the temperature range of 250–400 °C for pure nickel is critical, after which there is a sharp drop in mechanical properties. Nanoparticles at the grain boundaries of the matrix effectively prevent its deformation.

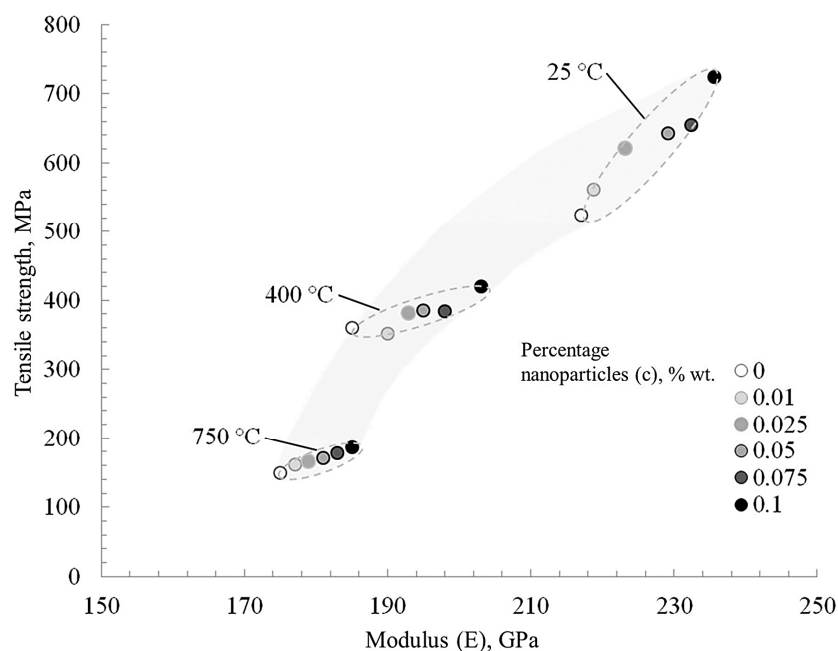


**Figure 12.** The change in the ultimate tensile strength and elastic modulus of nickel depends on nanofibers' concentration and the test temperature.

#### 4. Discussion

When nanofibers are added to nickel the general trend of increasing Young's modulus by 10% takes place (Figure 8). This is most likely due to the high surface energy of alumina nanofibers, which contributes to the development of contact with the matrix and a better adhesion.

The tensile strength of sintered nickel increases by 10–40% with an increase of the nanofibers' content in the range of 0.01–0.1 wt.% at room temperature. It is known that the temperature range of 250–400 °C for pure nickel is a turning point, after which a decrease of an extreme character occurs in the tensile strength (Figure 10).

The impurities formed during nanofibers' introduction strongly affect the adhesion between the grains in "pure" nickel and lead to the material strength changing. However, it is known that nickel grade 200 (99.6% Ni, 0.04% C) or 201 (99.6% Ni, 0.02% C maximum) [3] has a lower purity than PNK-UT3. However, that does not lead to a tensile strength increase above 750 °C and more. The tensile strength of the materials obtained in this work is higher than in the literature [29] by an average of 70 MPa. The influence of carbon impurities is ambiguous. It is noted in various works as a positive [32] and negative [33,34] effect on nickel cohesion.

According to the Obraztsov–Lurie–Belov micromechanical model [21], based on the gradient theory of elasticity, even small amounts of high-modulus particles that are introduced into a softer porous matrix promote the development of interparticle contacts in the matrix and a gradient change in the mechanical properties from the hard particles to the matrix. The formed layer between the particle and the matrix has higher strength properties than the matrix, which positively affects the strength of the entire material. This effect has been demonstrated on many materials [3,19–21].

The occurrence of barriers to the movement of dislocations in the form of added nanofibers slows down the deformation of the material, in this case along the grain boundaries. With an increase in the nanoparticles' concentration to 0.1 wt.%, the plasticity of the material decreases, but the tensile strength increases. The tensile strength tests of nickel materials are consistent with those previously obtained for nickel with bimodal grain size particles from 50 nm to 25  $\mu\text{m}$  [30,35].

The nanofibers have an uneven surface with convex and concave sections, chips, and a variable composition. This can lead to the introduction of voids in the interphase zone of



strengthening, leading to a state of nonequilibrium grain boundaries. In the early stages of sintering, nanoparticles contribute to shrinkage due to the introduction of additional defects and stresses, and on the other hand they prevent the coarsening of matrix grains in the late stages of consolidation. Nanopowders are nonequilibrium systems with an excess of free energy. The pressure resulting from a curved surface with two principal radii of curvature can exceed 300 MPa for particles with a size of 20 nm compared with 3 MPa for particles with a size of 1  $\mu\text{m}$  [36].

According to TEM images, the obtained nickel samples contain grains of submicron size, contributing to strengthening [2,21]. One might assume that there are oxide films on metal powders, including NiO on nickel, which can also inhibit nickel self-diffusion during sintering. If we rely on studies [37], a significant strengthening of nickel is provided with films with a thickness of 45–110 nm. The TEM results confirm that nickel oxide films at grain boundaries are minimal in our materials. It can be argued that in this case, their effect is not significant. The formation of chemical compounds between nickel oxide and alumina nanoparticles as alumina–nickel spinel  $\text{NiAl}_2\text{O}_4$  is not excluded [16,38,39]. However, TEM data did not totally confirm this.

In the literature [40], the properties and effect of Ni–NiO system composites' formation modes were investigated. It was found that the amount of nickel oxide in "natural" film did not affect the mechanical properties of nickel, incl. at a concentration of NiO of up to 1 wt.%. In the literature, [41] said that in order to form more than 0.5 wt.% NiO (in the Ni– $\text{Al}_2\text{O}_3$  system), it is necessary to make the process in the air (except at a high temperature of up to 800 °C with a holding time over 12 min). According to work [42] about the SPS sintering influence of nickel with a high alumina content, at a sintering temperature of 1200 °C for 10 min there was no noticeable nickel oxide formation. It should also be noted that the probability of the appearance of metal-to-metal contacts during spark plasma sintering at a pressure of more than 10 MPa makes it possible to destroy the film by analogy with aluminum [43,44]. The high temperature of pulsed discharges during SPS sintering can also lead to the dissociation of NiO. According to the literature [37], the oxygen pressure increases almost 160-fold for the reaction  $\text{NiO} \rightarrow \text{Ni} + \frac{1}{2}\text{O}_2$  with the temperature rising from 1127 °C to 1327 °C. The technology of composites obtaining in this work does not imply compliance with the conditions favorable for strengthening by oxide films' formation. Studies of the presence of nickel oxide  $\text{Ni}_2\text{O}_3$  cannot be accepted for these estimates since they are not confirmed by systematic studies and analytical methods [45,46].

As was established as a result of a sintered samples' microstructure TEM analysis, a small amount of free carbon was formed in the porous material during sintering, which could affect some hardening.

## 5. Conclusions

Nickel samples containing alumina nanofibers in the range of 0–0.1 wt.% were obtained by mechanical activation of powders with the subsequent addition of nanoparticles under the influence of ultrasound during mixing and spark plasma sintering. The microstructure TEM analysis shows that there are no nickel oxide films that could affect the material's mechanical properties. Nickel grains have an elongated shape with a length of more than 300 nm and a width of 50 nm. During spark plasma sintering in graphite form, some diffusion of carbon into nickel occurs, due to which pyrocarbon is formed at the grain boundaries. Nanofibers of aluminum oxide have different lengths and are located along the grain boundaries of the nickel matrix, incl. grasping the grains of metal.

The tensile strength of sintered nickel increases by 10–40% with an increase in the nanofibers' concentration to 0.1 wt.% at room temperature. With an increase of the tensile strength test temperature to 400–750 °C, the increase in strength is not so pronounced (5–10%) when compared with "pure" nickel. The nanoparticles affect the elastic properties of nickel, which increase by 10% in room temperature tests. Besides, it was noted that the nanofibers interfered with the softening of nickel when the test temperature was in the range of 400–750 °C.

Changes in the short-term tensile strength and Young's modulus dependent on the nanofibers' concentration and the test temperature have been shown. Increasing the nanofibers' concentration to the range of 0.01–0.1 wt.% leads to an increase in the mechanical properties of nickel of 50–100% depending on the test temperature (25–750 °C). Based on the analysis of the literature and the data obtained in this work, it can be assumed that the main effect on hardening is most likely due to the shape and size of the grains of nickel themselves and the addition of nanofibers of aluminum oxide. However, in the future it is necessary to assess the possible contribution of carbon that gets into nickel when sintering in graphite form.

**Author Contributions:** Conceptualization, V.K.; methodology, L.A.; software, L.A.; validation, S.S., B.I.; formal analysis, D.K., G.B., Y.S.; investigation, L.A., V.K., Z.E.; resources, L.A.; data curation, L.A.; writing—original draft preparation, L.A.; writing—review and editing, S.S.; visualization, L.A.; supervision, L.A.; project administration, L.A.; funding acquisition, L.A. All authors have read and agreed to the published version of the manuscript.

**Funding:** This research received no external funding by RFBR, project number 20-33-70009.

**Institutional Review Board Statement:** Not applicable.

**Informed Consent Statement:** Not applicable.

**Data Availability Statement:** In this section, please provide details regarding where data supporting reported results can be found, including links to publicly archived datasets analyzed or generated during the study. Please refer to suggested Data Availability Statements in section “MDPI Research Data Policies” at <https://www.mdpi.com/ethics>. You might choose to exclude this statement if the study did not report any data.

**Acknowledgments:** The authors thank Lurie S.A. for informative consultations and cooperation.

**Conflicts of Interest:** The authors declare no conflict of interest.

## References

1. Huebner, E.U. (Ed.) *Nickel Alloys*; Marcel Dekker Inc.: New York, NY, USA; Basel, Switzerland, 2000; 180p.
2. Goldshtein, M.I.; Litvinov, V.S.; Bronfin, M.F. *Metallophysics of High-Strength Alloys*; Metallurgia: Moscow, Russia, 1986; 312p.
3. Davis, J.R. (Ed.) *Nickel, Cobalt, and Their Alloys. ASM Speciality Handbook*; ASM International: Materials Park, Novelty, OH, USA, 2000; 400p.
4. Bruckart, W.L.; Jaffee, R.I. Cladding of molybdenum for service in air at elevated temperature. *Trans. Am. Soc. Met.* **1952**, *44*, 44.
5. Lurie, S.; Volkov-Bogorodskiy, D.; Solyaev, Y.; Rizahanov, R.; Agureev, L. Multiscale modelling of aluminium-based metal-matrix composites with oxide nano-inclusions. *Comput. Mater. Sci.* **2016**, *116*, 62–73. [[CrossRef](#)]
6. Kostikov, V.I.; Agureev, L.E.; Ereemeeva, Z.V. Development of nanoparticle-reinforced alumocomposites for rocket-space engineering. *Russ. J. Non Ferr. Met.* **2015**, *56*, 325–328. [[CrossRef](#)]
7. Sharma, A.; Roh, M.-H.; Jung, D.-H.; Jung, J.-P. Effect of ZrO<sub>2</sub> Nanoparticles on the Microstructure of Al-Si-Cu Filler for Low-Temperature Al Brazing Applications. *Met. Mater. Trans. A* **2016**, *47A*, 510–521. [[CrossRef](#)]
8. Chuvil'deev, V.N.; Kopylov, V.I.; Zeiger, W. A theory of non-equilibrium grain boundaries and its applications to nano- and micro-crystalline materials processed by ECAP. *Ann. Chim. Sci. Des Matériaux* **2002**, *27*, 55–64. [[CrossRef](#)]
9. Ohji, T.; Hirano, T.; Nakahira, A.; Niihara, K. Particle/Matrix interface and its role in creep inhibition in alumina silicon carbide nanocomposites. *J. Am. Ceram. Soc.* **1996**, *79*, 33–45. [[CrossRef](#)]
10. Grigorovich, V.K.; Sheftel', E.N. *Dispersion Hardening of Refractory Metals*; Nauka: Moscow, Russia, 1980; 304p.
11. Gottstein, G. *Physical Foundations of Materials Science*; Springer: Berlin, Germany, 2004; 502p.
12. Thompson, A.W. Substructure strengthening mechanisms. *Met. Trans.* **1977**, *8A*, 833–842. [[CrossRef](#)]
13. Lugovskoi, Y.F. Effect of structure on the fatigue strength of dispersion-hardened condensated based on copper II. Analysis of the first coefficient of the Mott—Stroh relation. *Powder Met. Met. Ceram.* **1998**, *37*, 432–437. [[CrossRef](#)]
14. Taira, S.; Otani, R. *Theory of High Temperature Strength of Materials*; Metallurgiya: Moscow, Russia, 1986; 280p.
15. Springer Nature. *Spark Plasma Sintering of Materials. Advances in Processing and Applications*; Springer Nature: Cham, Switzerland, 2019; 767p.
16. Borkar, T.; Banerjee, R. Influence of spark plasma sintering (SPS) processing parameters on microstructure and mechanical properties of nickel. *Mater. Sci. Eng. A* **2014**, *618*, 176–181. [[CrossRef](#)]
17. Zhao, Y.; Topping, T.; Bingert, J.F.; Thornton, J.; Dangelewicz, A.; Li, Y.; Liu, W.; Zhu, Y.; Zhou, Y.; Lavernia, E. High Tensile Ductility and Strength in Bulk Nanostructured Nickel. *Adv. Mater.* **2008**, *20*, 3028–3033. [[CrossRef](#)]

18. Naimi, F.; Minier, L.; Le Gallet, S.; Couque, H.; Bernard, F. Dense Nanostructured Nickel Produced by SPS from Mechanically Activated Powders: Enhancement of Mechanical Properties. *J. Nanomater.* **2013**, *11*. [[CrossRef](#)]
19. Agureev, L.E.; Kostikov, V.I.; Yeremeyeva, Z.V.; Barmin, A.A.; Rizakhanov, R.N.; Ivanov, B.S.; Ashmarin, A.A.; Laptev, I.N.; Rudshiteyn, R.I. Powder aluminum composites of Al–Cu system with micro-additions of oxide nanoparticles. *Inorg. Mater. Appl. Res.* **2016**, *7*, 507–510. [[CrossRef](#)]
20. Mironov, V.V.; Agureev, L.E.; Eremeeva, Z.V.; Kostikov, V.I. Effect of Small Additions of Alumina Nanoparticles on the Strength Characteristics of an Aluminum Material. *Dokl. Phys. Chem.* **2018**, *481*, 110–113. [[CrossRef](#)]
21. Lurie, S.; Belov, P.; Volkov-Bogorodsky, D.; Tuchkova, N. Interphase layer theory and application in the mechanics of composite materials. *J. Mater. Sci.* **2006**, *41*, 6693–6707. [[CrossRef](#)]
22. Saunders, Z.; Noack, C.W.; Dzombak, D.A.; Lowry, G. Characterization of engineered alumina nanofibers and their colloidal properties in water. *J. Nanoparticle Res.* **2015**, *17*, 1–14. [[CrossRef](#)]
23. Bravaya, N.M.; Galiullin, A.N.; Saratovskikh, S.L.; Panin, A.; Faingold, E.; Vasilev, S.G.; Bubnova, M.; Volkov, V. Synthesis and properties of hybrid materials obtained by in situ copolymerization of ethylene and propylene in the presence of Al<sub>2</sub>O<sub>3</sub> nanofibers (NAFEN™) on catalytic system rac-Et (2-MeInd) 2ZrMe<sub>2</sub>/isobutylalumoxane. *J. Appl. Polym. Sci.* **2016**. [[CrossRef](#)]
24. Panda, P.K.; Ramakrishna, S. Electrospinning of Alumina Nanofibers Using Different Precursors. *J. Mater. Sci.* **2007**, *42*, 2189–2193. [[CrossRef](#)]
25. Yang, C.; Huang, H.-F.; de los Reyes, M.; Yan, L.; Zhou, X.-T.; Xia, T.; Zhang, D.-L. Microstructures and Tensile Properties of Ultrafine Grained Ni- (1–3.5) wt.% SiCNP Composites Prepared by a Powder Metallurgy Route. *Acta Met. Sin.* **2015**, *28*, 809–816. [[CrossRef](#)]
26. Maweja, K.; Phasha, M.; Yamabe-Mitarai, Y. Alloying and microstructural changes in platinum–titanium milled and annealed powders. *J. Alloy. Compd.* **2012**, *523*, 167–175. [[CrossRef](#)]
27. Rosenberg, S.J. *Nickel and Its Alloys*; National Bureau of Standards Monograph: Washington, DC, USA, 1968; 106p.
28. Farraro, R.; McLellan, R.B. Temperature dependence of the Young's modulus and shear modulus of pure nickel, platinum, and molybdenum. *Metall. Trans. A* **1977**, *8*, 1563–1565. [[CrossRef](#)]
29. *Engineering Properties of Nickel 200 and 201, Technical Bulletin T-15*; Huntington Alloy Products Division, The International Nickel Co. Inc.: Paramus, NJ, USA, 1964.
30. *Nickel. Circular of the Bureau of Standarts. No. 100*; Washington Government Printing Office: Washington, DC, USA, 1921; 105p.
31. Bollmann, W. Electron-microscopic observations on the recrystallization of nickel. *J. Inst. Met.* **1959**, *87*, 439.
32. Masatake, Y.; Motoyuki, S.; Hideo, K. Energetics of segregation and embrittling potency for non-transition elements in the Ni Σ5 (012) symmetrical tilt grain boundary: A first-principles study. *J. Phys. Condens. Matter.* **2004**, *16*, 3933. [[CrossRef](#)]
33. Sanyal, S.; Waghmare, U.V.; Subramanian, P.R.; Gigliotti, M.F.X. Effect of dopants on grain boundary decohesion of Ni: A first-principles study. *Appl. Phys. Lett.* **2008**, *93*. [[CrossRef](#)]
34. Young, G.; Najafabadi, R. *Applications of Ab Initio Modeling to Materials Science: Grain Boundary Cohesion and Solid State Diffusion*; No. LM-04K037; Lockheed Martin Corporation: Owego, NY, USA, 2004.
35. Hanlon, T.; Kwon, Y.-N.; Suresh, S. Grain size effects on the fatigue response of nanocrystalline metals. *Scr. Mater.* **2003**, *49*, 675–680. [[CrossRef](#)]
36. Ragulya, A.V.; Skorokhod, V.V. *Consolidated Nanostructured Materials*; Naukova dumka: Kiev, Ukraine, 2007; 369p.
37. Ramakrishnan, P.; Tendolkar, G.S. Influence of thin oxide films on the mechanical properties of sintered metal-powder compacts. *Powder Metall.* **1964**, *7*, 34–49. [[CrossRef](#)]
38. Bhattacharjee, P.P.; Sinha, S.K.; Upadhyaya, A. Effect of sintering temperature on grain boundary character distribution in pure nickel. *Scr. Mater.* **2007**, *56*, 13–16. [[CrossRef](#)]
39. Minier, L.; Le Gallet, S.; Grin, J.; Bernard, F. A comparative study of nickel and alumina using spark plasma sintering (SPS). *Mater. Chem. Phys.* **2012**, *134*, 243–253. [[CrossRef](#)]
40. Takagi, H.; Nishiyama, Y.; Sakamaki, K.; Yoshida, K. Microstructure and Hardness of Ni-NiO Composites Prepared by Powder Metallurgy. *Trans. Jpn. Soc. Mech. Eng. Ser. A* **1995**, *6*, 1933–1939. [[CrossRef](#)]
41. Fujimura, T.; Tanaka, S.-I. In-situ high temperature x-ray diffraction study of Ni/Al<sub>2</sub>O<sub>3</sub> interface reactions. *Acta Mater.* **1997**, *45*, 4917–4921. [[CrossRef](#)]
42. Voicu, C.; Popa, F.; Marinca, T.F.; Neamtu, B.V.; Lostun, M.; Lupu, N.; Chicinas, I. Synthesis and characterisation of Al<sub>2</sub>O<sub>3</sub>/Ni-type composites obtained by spark plasma sintering. *Powder Metall.* **2018**. [[CrossRef](#)]
43. Xie, G.; Ohashi, O.; Song, M.; Furuya, K.; Noda, T. Behavior of oxide film at the interface between particles in sintered Al powders by pulse electric-current sintering. *Metall. Mater. Trans. A* **2003**, *34A*, 699–703. [[CrossRef](#)]
44. Nagae, T.; Yokota, M.; Nose, M.; Tomida, S.; Kamiya, T.; Saji, S. Effects of pulse current on an aluminum powder oxide layer during pulse current pressure sintering. *Mater. Trans.* **2002**, *43*, 1390–1397. [[CrossRef](#)]
45. Dagan, G.; Shen, W.-M.; Tomkiewicz, M. Passivation of Permalloy Thin Films: II. In Situ Characterization of the Oxide Layer by Photoelectrochemical and Impedance Measurements. *J. Electrochem. Soc.* **1992**, *139*, 1855–1861. [[CrossRef](#)]
46. Sikora, E.; Macdonald, D.D. Nature of the passive film on nickel. *Electrochim. Acta* **2002**, *48*, 69–77. [[CrossRef](#)]